

Nanostructure of β -type titanium alloys through severe plastic deformation

Hakan Yilmazer^{1*}, Mitsuo Niinomi¹, Ken Cho¹, Masaaki Nakai¹, Junko Hieda¹, Shigeo Sato¹, and Yoshikazu Todaka²

¹Institute for Materials Research, Tohoku University, Sendai 980-8577, Japan

²Department of Production Systems Engineering, Toyohashi University of Technology, Toyohashi 441-8580, Japan

*Corresponding author. Tel: (+81) 22 215 2081; E-mail: hakan@imr.tohoku.ac.jp

Received: 26 August 2013, Revised: 29 September 2013 and Accepted: 18 October 2013

ABSTRACT

A novel β -type titanium alloy Ti-29Nb-13Ta-4.6Zr (TNTZ) has been developed and extensively researched to achieve highly desirable mechanical properties such as a high strength while maintaining a low Young's modulus that is close to that of bone, as an alternative candidate for conventional titanium metallic biomaterials such as Ti-6Al-4V ELI. Therefore, strengthening by grain refinement and increasing dislocation density is expected to provide TNTZ high mechanical strength while keeping a low Young's modulus because they keep the original β phase. In this case, severe plastic deformation, such as high-pressure torsion (HPT) processing, is a potential treatment for obtaining these properties. Furthermore, HPT processing is effective for producing ultrafine-grained TNTZ having high dislocation density in single β structure. The obtained promising results, which are a tensile strength of around 1100 MPa and a Young's modulus of around 60 GPa, motivated that the above mentioned mechanical properties can be achieved by microstructural refinement through HPT processing. However, the mechanism of microstructural refinement is unclear for TNTZ during HPT processing. Therefore, the aim of this study is to investigate microstructural changes of TNTZ through HPT processing by X-ray diffraction analysis and transmission electron microscopy. The microstructures of TNTZ subjected to cold rolling (TNTZ_{CR}) and HPT processing (TNTZ_{HPT}) comprised single β grains; however, the intense β {110} peak reveals that the preferred orientation is β <110> for TNTZ_{HPT}. While the microstructure of TNTZ_{CR} shows a comparatively high dislocation density ($2.3 \times 10^{16} \text{ m}^{-2}$), HPT processing leads to a drastic accumulation of dislocations ($5.3 \times 10^{16} \text{ m}^{-2}$ in dislocation density). Dislocations in the microstructures of TNTZ_{HPT} are well arranged for the cell wall and/or subgrain boundaries, with a stronger dipole character than random distribution. The dislocation density, arrangement parameter and crystallite diameter (around 11 nm) of TNTZ_{HPT} saturate from the center to the peripheral region of a coin shaped specimen at $N = 20$. Therefore, such a microstructural saturation in a specific strain inducing, $N = 20$, suggests a threshold for further investigation of β -type titanium alloys. Copyright © 2014 VBRI press.

Keywords: β -Type titanium alloy; high-pressure torsion; microstructural refinement; dislocation generation degradation.

Introduction

An excellent combination of great strength and low Young's modulus has been aimed for metallic materials used in structural implants that replace hard tissue [1]. When Young's modulus of the metallic implant and that of the bone are different, stress transfer becomes non-homogeneous between a metallic implant and a bone. Moreover bone atrophy is likely to occur and can lead to loosening of the metallic implant and re-fracturing of the bone by stress shielding effect which stimulation of stress towards the bone is reduced when the metallic implant has much higher Young's modulus such as 110 GPa for Ti-6Al-4V (Ti64) ELI [2, 3] than that of bone (10–30 GPa) [1].

A novel β -type titanium alloy, Ti-29Nb-13Ta-4.6Zr (TNTZ), with a low Young's modulus (~60 GPa) [2], relatively closer to that of bone (10–30 GPa) as compared with conventional titanium biomaterials such as Ti64 ELI,

has been developed [4]. Microstructural features, including grain size, the state of grain boundaries, and lattice defects, play a major role in improving the desired balance between strength and Young's modulus of TNTZ. However conventional process such as solution treatment (ST), cold rolling (CR), aging treatment (AT) are not sufficient to achieved a great strength while maintaining low Young's modulus as compared with Ti64 ELI (Fig. 1)[2].

Recently, severe plastic deformation (SPD) [5] such as high-pressure torsion (HPT) [6] is a proven technique for inducing a very intense plastic strain to form a microstructure composed of ultrafine-grained (100–500 nm) or nanostructured (<100 nm) grain in metallic materials. The basic principle of HPT processing is that a bulk material is deformed by a very intense torsional strain without introducing any significant changes in the overall dimensions of the work-piece. Such metallic materials show

great mechanical strength as compared that of the coarse grained materials [5, 6].

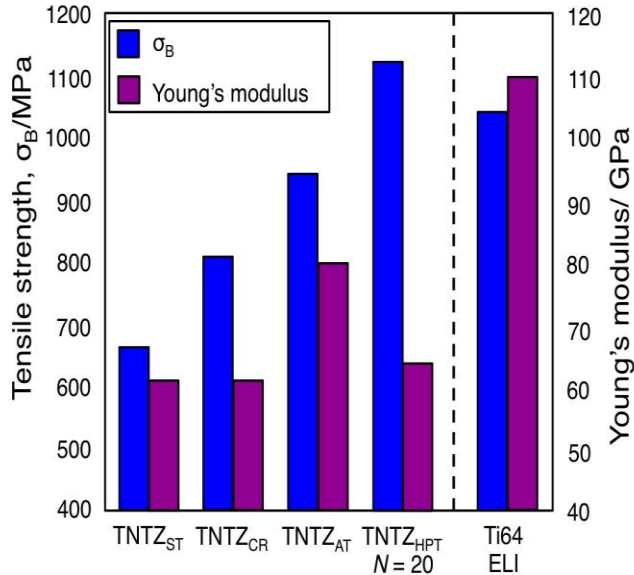


Fig. 1. Tensile strengths and Young's moduli of TNTZ subjected to solution treatment (ST), cold rolling (CR), aging treatment (AT), HPT processing, and Ti64 ELI.

In order to obtain the desired mechanical properties, microstructural refinement of TNTZ using HPT processing has been studied [7]. It is found that HPT processing is effective for producing ultrafine-grains in a single β structure of TNTZ [7]. Furthermore, such TNTZ subjected to HPT processing shows a remarkable mechanical biocompatibility; which is a high mechanical strength (around 1100 MPa) and while maintaining a low Young's modulus (around 60 GPa) (Fig. 1) [8]. However, the mechanisms of dislocation generation and microstructural refinement are unclear for β -type titanium alloys having BCC structure during HPT processing even though it is extensively investigated and clearly shown for FCC metals such as Al [9], Ni [10], Cu [11] and their alloys. Therefore, It has been aimed to clear microstructural refinement mechanism of TNTZ through HPT processing that it can shed light on further investigations for β -type titanium alloys and relatively BCC metals in order to improve their mechanical, physical and chemical properties. Therefore, the microstructure of TNTZ subjected to HPT processing has been investigated using X-ray line profile analysis, and transmission electron microscopy in this study.

Experimental

Material

The chemical composition of the hot-forged Ti-29Nb-13Ta-4.6Zr (TNTZ) bar, which was maintained from Daido Steel Company, used in this study is shown in Table 1.

Material preparation

TNTZ bar with a length of 50 mm and a diameter of 25 mm was subjected to solution treatment at 1063 K for 3.6 ks under vacuum followed by water quenching. And then, solutionized TNTZ bar was cold rolled to plates with a

thickness of 0.85 mm by a reduction ratio of more than 80% (TNTZ_{CR}). Finally, the TNTZ_{CR} plates were machined into coin-shaped specimens with a thickness of 0.85 mm and a diameter of 20 mm for high-pressure torsion (HPT) processing.

Table 1. Chemical composition of Ti-29Nb-13Ta-4.6Zr (TNTZ).

Elements	Nb	Ta	Zr	C	N	O	H	Fe	Ti
Mass [%]	28.6	12.3	4.75	0.02	0.01	0.09	0.04	0.22	bal.

HPT processing

The coin-shaped specimens of TNTZ_{CR} were subjected to HPT processing (TNTZ_{HPT}) using a pair of anvils, which the lower anvil of HPT machine was rotated for numbers (N) of 20 at a rotational speed of 0.2 rpm under a pressure of about 1.25 GPa at room temperature (298 K). The equivalent strain, ε_{eq} , is given by the following equation [6]:

$$\varepsilon_{eq} = \frac{2\pi r N}{t\sqrt{3}} \quad (1)$$

where r is the distance from the specimen center, π is the ratio of the circumference of a circle to its diameter, and t is the specimen thickness. Hereafter, each coin-shaped specimen of TNTZ_{CR} subjected to HPT processing is referred to as TNTZ_{HPT}.

Material characterization

The microstructures of TNTZ_{CR} and TNTZ_{HPT} were examined by X-ray diffractometry (XRD) and transmission electron microscopy (TEM). The phase constitution was analyzed by XRD using Cu-K α radiation with a voltage of 40 kV and a current of 40 mA for TNTZ_{CR} and TNTZ_{HPT} respectively in the center ($R/0$), the half-radius position ($R/2$), and near the edge (R) where R is the radius of the coin-shaped specimen.

In addition, TEM observations were carried out with an accelerating voltage of 200 kV at the $R/2$ position on the cross section of the coin-shaped specimen. Details of the TEM sample preparation from a cross section are explained in a previous study [7]. For TEM observations from cross section, the half specimen of TNTZ_{HPT} was adhered between two silicon substrates by epoxy from surface and then cut to a thin slice as parallel to cross section near the diameter of TNTZ_{HPT}. It was wet polished to the thickness below 50 μ m using water-proof emery papers of up to #4000 and were then buff polished to obtain the mirror surface by colloidal SiO₂ suspension. Subsequently, a copper ring with 3 mm diameter was adhered on the polished slices at r_h position by epoxy. Subsequently it was further thinned using a dimple grinder and an ion milling.

X-ray line profile analysis (XLPA)

The XRD profiles have been evaluated by XLPA [12] using the convolutional multiple whole profile (CMWP) fitting method [13-15]. The measured XRD profiles fitted by

CMWP using a convolution profile (I) of the theoretical profiles of size profile, I_s , as a function of the size of crystallite, which is the smallest unit of a crystal aggregation, microstrain profile (I_m) and the instrumental profile (I_i):

$$I = I_m + I_s + I_i \quad (2)$$

The size profile (I_s) is determined by median, m , and logarithmic variance, σ , of log-normal size distribution function. Then, the average crystallite diameter ($\langle x \rangle_{\text{area}}$) is calculated [13] as:

$$\langle x \rangle_{\text{area}} = m \exp(2.5\sigma^2) \quad (3)$$

In addition to the size profile, the corresponding strain profile function (I_m) used in CMWP fitting is given by its Fourier transform derived as [16, 17]:

$$I_m = \exp\left(-2\pi^2 g^2 L^2 \langle \varepsilon_{g,L}^2 \rangle\right) \quad (4)$$

where g is the absolute value of the diffraction vector, L is Fourier variable, and $\langle \varepsilon^2 \rangle$ is mean square strain defined as:

$$\langle \varepsilon_{g,L}^2 \rangle = \frac{\rho C b^2}{4\pi} f(L/R_e) \quad (5)$$

where ρ , C , b , and R_e are the dislocation density, the contrast factor of dislocations, the absolute value of the Burgers vector, and the effective outer cut-off radius of dislocations, respectively. Also, the dislocation arrangement parameter (M) can be introduced by Wilkens et al. [17] as

$$M = R_e \sqrt{\rho} \quad (6)$$

where R_e is the effective radius of dislocations and ρ is the dislocation density. If the M parameter is smaller than unity ($M \ll 1$), then correlation between the dislocations is strong. On the other hand, if the value of M parameter is larger than unity ($M \gg 1$), then dislocations are randomly distributed in grains.

Results and discussion

The microstructures of TNTZ_{CR} and TNTZ_{HPT} have been demonstrated by (XLPA) using CMWP fitting method. **Figs. 2** and **3** show the measured patterns (marked by open circles) of TNTZ_{CR} and TNTZ_{HPT}, the patterns fitted by the CMWP fitting method (marked by red line), the difference between the measured and fitted data (marked by blue line), and the background baseline (marked by green line) at the bottom of the profiles, representatively.

The Differences between the measured and fitted profiles are plotted at the bottom of the figure. TNTZ_{CR} and TNTZ_{HPT} comprise of a single β microstructure, as shown in **Figs. 2** and **3**. However, while the β {110} peak becomes more intense through HPT processing, the β {200} and β {211} peaks become less intense. The intense β {110} peak

reveals that the preferred orientation is β <110> because of HPT processing of TNTZ. Furthermore, the XRD profile shows that the diffraction peaks broaden after HPT processing. The broadened diffraction profiles of TNTZ_{HPT} indicate that the microstructure is composed of very small grains and subgrains with relatively large microstrain [18] due to the accumulation of dislocations formed by HPT processing [6].

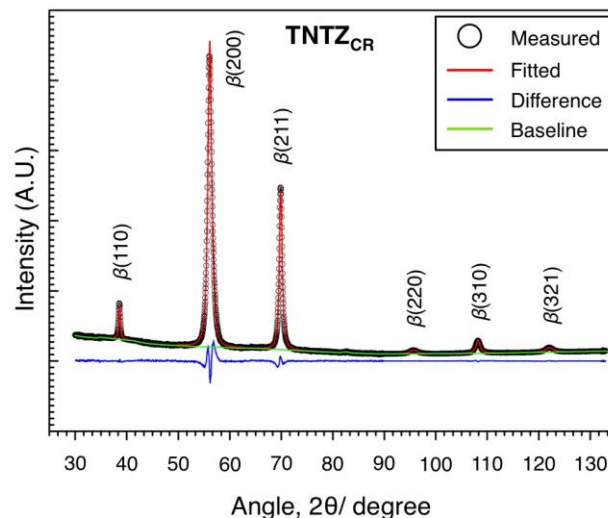


Fig. 2. Measured (open circles) and theoretical fitted (red line) intensity profiles of TNTZ_{CR} with baseline (green line).

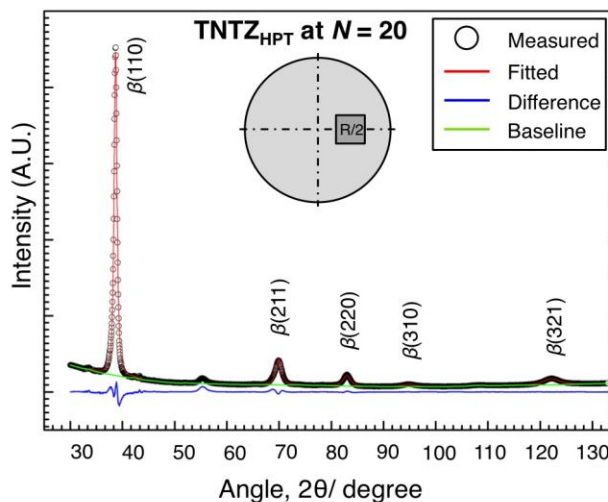


Fig. 3. Measured (open circles) and theoretical fitted (red line) intensity profiles of TNTZ_{HPT} at $R/2$ position with baseline (green line). Differences between the measured and fitted profiles are plotted at the bottom of the figure.

Figs. 4 and **5** show the dislocation characteristics such as density (ρ) and arrangement parameter (M), and the crystallite diameter (D), which indicates the diameters of subgrains and/or dislocation cells, estimated by CMWP fitting, of TNTZ_{CR} and on from $R/0$, $R/2$, and R positions of TNTZ_{HPT}. TNTZ_{CR} exhibits a comparatively high dislocation density ($2.3 \times 10^{16} \text{ m}^{-2}$) [19] with a dislocation arrangement parameter of around 0.2. The M parameter, which is smaller than unity, suggests that dislocations are well arranged for the cell wall and/or subgrain boundaries

by the severe cold rolling. In addition, the crystallite diameter is around 18 nm for TNTZ_{CR} as shown in Fig. 5.

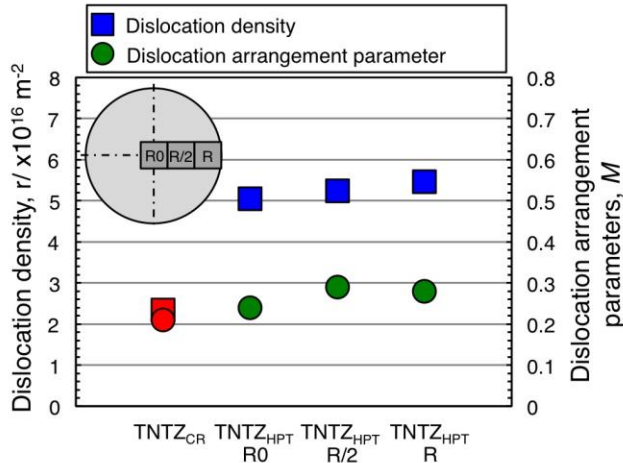


Fig. 4. Dislocation densities (ρ) and dislocation arrangement parameter (M) of TNTZ_{CR} and TNTZ_{HPT} with an illustration of analyzed position on coin-shaped specimen.

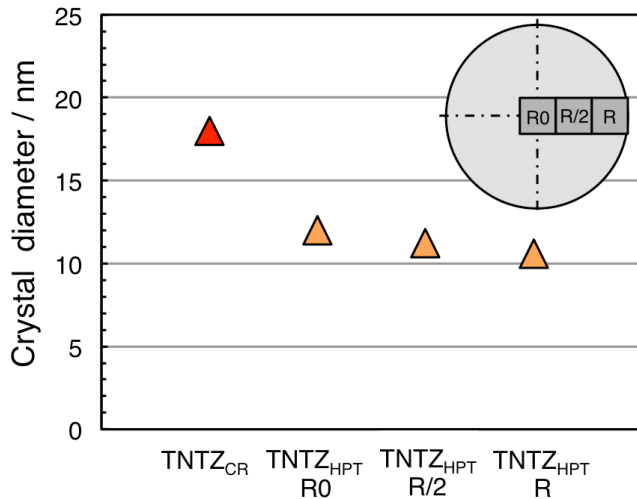


Fig. 5. Crystallite diameters of TNTZ_{CR} and TNTZ_{HPT} with an illustration of analyzed position on coin-shaped specimen.

The HPT processing leads to a drastic increase in dislocation density, which indicates a very large accumulation of dislocations during HPT processing as shown in Fig. 4. The dislocations generated during HPT processing accumulate in grains, due to being trapped by some hindrances such as boundaries and other dislocations. Then, the further deformation leads that a large number of dislocations arrange to form dislocation cells surrounded by thick walls. At the same time, the crystallite diameter decreases in the β grains of TNTZ_{HPT} (Fig. 5). Eventually, the cell walls should evolve by totally annihilation of dislocations so that the fine grains forms grain boundaries having high angles of misorientation as deformation continues [10, 20]. The M parameters (around 0.24) of TNTZ_{HPT} suggest a strong dipole character. The dipole character of dislocations is usually increasing with the dislocation density. Therefore, the decreasing tendency of M parameter with increasing dislocation density indicates a good correlation between these two quantities. However,

the dislocation density and crystallite diameter saturate to around to $5.3 \times 10^{16} \text{ m}^{-2}$ with distance from center to peripheral regions for $N = 20$, which the equivalent strain increases with distance from center (Eq.1). The saturation of dislocation density with increasing strain indicates [21] that, the annihilation of dislocations is more difficult and consequently microstructural refinement is slower and limited for TNTZ_{HPT} than those of some metals such as Al [9], Ni [10], Cu [11] and their alloys subjected to SPD techniques. As contrary, microstructural evolution occurs slowly in most of BCC metals such as Mo [22], Cr [23], and W [24] owing to the lower stacking fault energies. Therefore, higher strain should be imposed on TNTZ to achieve microstructural homogeneity.

Figs. 6 and 7 show bright-field images of TNTZ_{CR} and TNTZ_{HPT} at $R/2$. Grain boundaries are well defined in the microstructure of TNTZ_{CR} after severe cold rolling with a reduction ratio of over 80%.

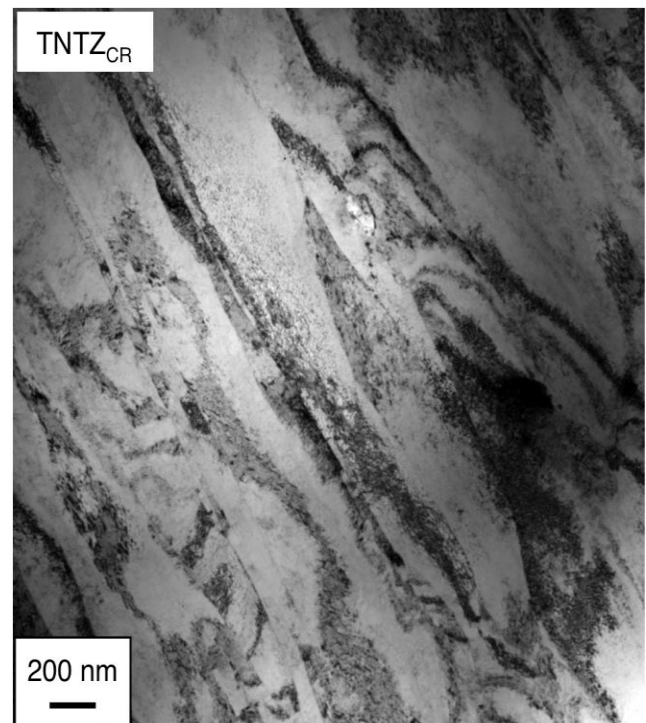


Fig. 6. TEM bright field image of TNTZ_{CR}.

It is reported that the TNTZ_{HPT} shows an ultrafine microstructure consisting of elongated grains with a length of around 300 nm and a width of around 45 nm that it can be also observed in Fig. 7. Furthermore, the bright field image of TNTZ_{HPT} at $R/2$ in Fig. 7 shows that subgrains or/and dislocation cells in grains exhibit blurred, and wavy boundaries. These boundaries indicates the presence of exterior dislocations which do not play a part in the formation of misorientation at boundaries of the grains and the subgrains or/and dislocation cells in grains of TNTZ_{HPT}. The exterior dislocations densities on the boundaries lead higher internal strain energies. Such boundaries are called as non-equilibrium boundaries [25, 26], which are reported in several HPT experiments [6, 27]. On the other hand, the contrast in the bright field image shows well-arranged dislocations for dislocation cells and subgrains.

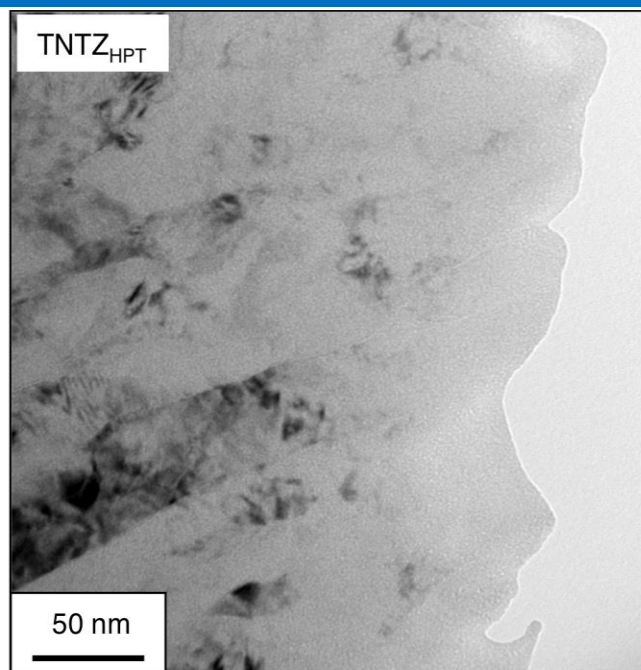


Fig. 7. TEM bright field image of TNTZ_{HPT} at R/2.

The hardness distributions in the radial direction on the surfaces and cross sections of TNTZ_{HPT} were reported in previous study [8]. The hardness distribution of TNTZ_{HPT} exhibits some variation on the surface and cross sections. The hardness distributions confirm that, the hardness increases with the distance from the center of TNTZ_{HPT} due to the heterogeneous microstructure of TNTZ at $N < 20$. Further, hardness distribution clearly saturates around 300 HV at $N \geq 20$. Further, the hardness of TNTZ_{HPT} in the central region increases subsequently, and it saturates at $N \geq 20$. These results provide clear evidence for the achievement of a homogeneous microstructure in TNTZ_{HPT} at $N = 20$. Furthermore, the saturations of dislocation density, arrangement parameter, and crystallite diameter (around 11 nm) exhibit homogeneity of microstructure from center to the peripheral region of TNTZ_{HPT} at $N = 20$, which is consistent with saturation of mechanical behaviors.

Conclusion

The microstructural evolution of β -type Ti–29Nb–13Ta–4.6Zr (TNTZ) through high-pressure torsion (HPT) processing for biomedical applications has been investigated in this study. The following results were obtained:

- TNTZ_{CR} and TNTZ_{HPT} are comprised of a single β microstructure. However, the intense β {110} peak reveals that the preferred orientation is β <110> for TNTZ because of HPT processing.
- The microstructure of TNTZ_{CR} shows a comparatively high dislocation density ($2.3 \times 10^{16} \text{ m}^{-2}$). The HPT processing leads to a drastic increase in dislocation density ($5.3 \times 10^{16} \text{ m}^{-2}$) due to a very large accumulation of dislocations.
- Dislocations are well arranged for the cell wall and/or subgrains boundaries, and in a stronger dipole character

than random distribution in the microstructures of TNTZ_{CR} and TNTZ_{HPT}

- The dislocation density, dislocation arrangement parameter and crystallite diameter of TNTZ_{HPT} at $N = 20$ are saturated from the center to the peripheral region of the coin shaped specimen.

Acknowledgements

This study was supported in part by Grant-in-Aid for Scientific Research (A) No.24246111 and Grant-in-Aid for Young Scientists (B) No. 25820367 from the Japan Society for the Promotion of Science, Innovation Research for Biosis-Abiosis Intelligent Interface” of the Ministry of Sports, Culture, and Education, Japan. Inamori Grants from the Inamori Foundation, Japan, and Titanium Research Grant from the Japan Titanium Society, Japan.

Reference

- Niinomi, M. *J. Mech. Behav. Biomater.* **2008**, *1*, 30.
DOI: [10.1016/j.jmbbm.2007.07.001](https://doi.org/10.1016/j.jmbbm.2007.07.001)
- Akahori, T.; Niinomi, M.; Fukui, H.; Suzuki, A. *J. Mater. Trans.* **2004**, *45*, 1540.
- Kuroda, D.; Niinomi, M.; Morinaga, M.; Kato, Y.; Yashiro, T. *Mater. Sci. Eng. A* **1998**, *243*, 244.
DOI: [10.1016/S0921-5093\(97\)00808-3](https://doi.org/10.1016/S0921-5093(97)00808-3)
- Akahori, T.; Niinomi, M.; Fukui, H.; Ogawa, M.; Toda, H. *Mater. Sci. Eng. C* **2005**, *25*, 248.
DOI: [10.1016/j.msec.2004.12.007](https://doi.org/10.1016/j.msec.2004.12.007)
- Valiev, R. Z.; Islamgaliev, R. K.; Alexandrov, I. V. *Prog. Mater. Sci.* **2000**, *45*, 103.
DOI: [10.1016/S0079-6425\(99\)00007-9](https://doi.org/10.1016/S0079-6425(99)00007-9)
- Zhilyaev, A. P.; Langdon, T. G. *Prog. Mater. Sci.* **2008**, *53*, 893.
DOI: [10.1016/j.pmatsci.2008.03.002](https://doi.org/10.1016/j.pmatsci.2008.03.002)
- Yilmazer, H.; Niinomi, M.; Nakai, M.; Hieda, J.; Todaka, Y.; Akahori, T.; Miyazaki, T. *J. Mech. Behav. Biomed. Mater.* **2012**, *10*, 235.
DOI: [10.1016/j.jmbbm.2012.02.022](https://doi.org/10.1016/j.jmbbm.2012.02.022)
- Yilmazer, H.; Niinomi, M.; Nakai, M.; Cho, K.; Hieda, J.; Todaka, Y.; Miyazaki, T. *Mater. Sci. Eng. C* **2013**, *33*, 2499.
DOI: [10.1016/j.msec.2013.01.056](https://doi.org/10.1016/j.msec.2013.01.056)
- Zhilyaev, A. P.; Oh-ishi, K.; Langdon, T. G.; McNelley, T. R. *Mater. Sci. Eng. A* **2005**, *410–411*, 277.
DOI: [10.1016/j.msea.2005.08.044](https://doi.org/10.1016/j.msea.2005.08.044)
- Zhilyaev, A. P.; Lee, S.; Nurislamova, G. V.; Valiev, R. Z.; Langdon, T. G. *Scripta Mater.* **2001**, *44*, 2753.
DOI: [10.1016/S1359-6462\(01\)00955-1](https://doi.org/10.1016/S1359-6462(01)00955-1)
- Horita, Z.; Langdon, T. G. *Mater. Sci. Eng. A* **2005**, *410–411*, 422.
DOI: [10.1016/j.msea.2005.08.133](https://doi.org/10.1016/j.msea.2005.08.133)
- Li, L.; Ungar, T.; Wang, Y. D.; Fan, G. J.; Yang, Y. L.; Jia, N.; Ren, Y.; Tichy, G.; Lendvai, J.; Choo, H.; Liaw, P. K. *Scripta Mater.* **2009**, *60*, 317.
DOI: [10.1016/j.scriptamat.2008.10.031](https://doi.org/10.1016/j.scriptamat.2008.10.031)
- Ribarik G. *Modeling of diffraction patterns based on microstructural properties, in Department of Materials Physics, Eotvos Lorand University, Budapest*, **2008** pp. 42–72.
- Ribárik, G.; Gubicza, J.; Ungár, T. *Mater. Sci. Eng. A* **2004**, *343*, 387.
DOI: [10.1016/j.msea.2004.01.089](https://doi.org/10.1016/j.msea.2004.01.089)
- Ungár, T.; Tichy, G.; Gubicza, J.; Hellmig, R. J. *J. Powder Diffr.* **2005**, *20*, 366.
DOI: [10.1063/1.3622333](https://doi.org/10.1063/1.3622333)
- Ungár, T.; Tichy, G. *Phys. Stat. Sol. A* **1999**, *171*, 425.
Wilkens, M. *Theoretical aspects of kinematical X-ray diffraction profiles from crystals containing dislocation distributions*, Fundamental Aspects of Dislocation Theory, Simmons, J. A.; Wit, R. de; Bullough, R. (Eds); Nat. Bur. Stand. (US) Spec. Publ. No. 317. : USA, **1970**, *2*, pp. 1195–1221.
- Balogh, L.; Ungar, T.; Zhao, Y.; Zhu, Y. T.; Horita, Z.; Xu, C.; Langdon, T. G. *Acta Mater.* **2008**, *56*, 809.
DOI: [10.1016/j.actamat.2007.10.053](https://doi.org/10.1016/j.actamat.2007.10.053)
- Kolobov, Yu. R.; Kieback, B.; Ivanov, K. V.; Weissgaerber, Th.; Girsova, N. V.; Pochivalov, Yu. I.; Grabovetskaya, G. P.; Ivanov, M. B.; Kazyhanov, V. U.; Alexandrov, I. V. *Int. J. Refract. Met. Hard Mater.* **2003**, *21*, 69.
DOI: [10.1016/S0263-4368\(03\)00002-7](https://doi.org/10.1016/S0263-4368(03)00002-7)

19. Wadsack, R.; Pippan, R.; Schedler, B. *Fusion Eng. Des.* **2003**, 265, 66–68.
DOI: [10.1016/S0920-3796\(03\)00136-4](https://doi.org/10.1016/S0920-3796(03)00136-4)
20. Wei, Q.; Zhang, H. T.; Schuster, B. E.; Ramesh, K. T.; Valiev, R. Z.; Kecskes, L. J.; Dowding, R. J.; Magness, L.; Cho, K. *Acta Mater.* **2006**, 54, 4079.
DOI: [10.1016/j.actamat.2006.05.005](https://doi.org/10.1016/j.actamat.2006.05.005)
21. Ungar, T. *Scrip. Mater.* **2004**, 51, 777.
DOI: [10.1016/j.scriptamat.2004.05.007](https://doi.org/10.1016/j.scriptamat.2004.05.007)
22. Winther, G.; Huang, X.; Godfrey, A.; Hansen, N. *Acta Mater.* **2004**, 52, 4437.
DOI: [10.1016/j.actamat.2004.05.050](https://doi.org/10.1016/j.actamat.2004.05.050)
24. Fischer, F. D.; Svoboda, J.; Appel, F.; Kozeschnik, E. *Acta Mater.* **2011**, 59, 3463.
DOI: [10.1016/j.actamat.2011.02.020](https://doi.org/10.1016/j.actamat.2011.02.020)
25. Valiev, R. Z. *Nat. Mater.* **2004**, 3, 511.
DOI: [10.1038/nmat1180](https://doi.org/10.1038/nmat1180)
26. Starink, M. J.; Qiao X. G.; Zhang, J.; Gao, N. *Acta Mater.* **2009**, 57, 5796.
DOI: [10.1016/j.actamat.2009.08.006](https://doi.org/10.1016/j.actamat.2009.08.006)
27. Divinski, S. V.; Reglitz, G.; Rosner, H.; Estrin, Y.; Wilde, G. *Acta Mater.* **2011**, 59, 1974.
DOI: [10.1016/j.actamat.2010.11.063](https://doi.org/10.1016/j.actamat.2010.11.063)

Advanced Materials Letters

Publish your article in this journal

[ADVANCED MATERIALS Letters](#) is an international journal published quarterly. The journal is intended to provide top-quality peer-reviewed research papers in the fascinating field of materials science particularly in the area of structure, synthesis and processing, characterization, advanced-state properties, and applications of materials. All articles are indexed on various databases including [DOAJ](#) and are available for download for free. The manuscript management system is completely electronic and has fast and fair peer-review process. The journal includes review articles, research articles, notes, letter to editor and short communications.

